

Dynamics of coupled piezoelectric energy harvesters*

Albert Granados[†]

Abstract

In this article we consider an energy harvesting device given by the coupling of two piezoelectric oscillators. We write the system as two coupled duffing equations (which model the mechanical part of the piezoelectric beams) plus a perturbation. The latter includes both the coupling between the beams (which is purely dissipative) and the periodic forcing, from which the device aims to absorb energy.

The non-perturbed system possesses a Normally Hyperbolic Manifold of dimension 4, with 6 and 5-dimensional stable and unstable manifolds, respectively. We apply the parameterization method to study the inner dynamics and evidence of heteroclinic connections when the perturbation is switched on.

Keywords: damped oscillators, parameterization method, normally hyperbolic manifolds.

Contents

1	Introduction	2
2	Invariant objects	6
2.1	Unperturbed system	6
2.2	Persistence of manifolds	15

*This work has been partially supported by MINECO MTM2015-65715-P Spanish grant and Marie Curie FP7 COFUND Ørsted fellowship. We acknowledge the use of the UPC Dynamical Systems group's cluster for research computing (<https://dynamicalsystems.upc.edu/en/computing/>)

[†]algr@dtu.dk, Department of Applied Mathematics and Computer Science, Technical University of Denmark, Building 303B, 2800 Kgs. Lyngby, Denmark.

3	Numerical framework for the parameterization method	16
3.1	A Newton-like method	17
3.1.1	First step: correction of the manifold and the inner dynamics	18
3.1.2	Second step: normal bundle correction	20
3.2	Computation of bundles, maps and frames for the unper- turbed case	21
4	Numerical results	25
4.1	Conservative case	25
4.2	Dissipative case	30
4.2.1	Weak damping	30
4.2.2	Weak dissipative coupling	31

1 Introduction

Energy harvesting systems consists of devices able to absorb energy from the environment and, typically, electrically power a load or accumulate electrical energy in accumulators (super capacitors or batteries) for later use. One of the most extended approaches is by means of piezoelectric materials, which, under a mechanical strain, generate an electric charge. Such materials are however mostly observed working in the inverse way in, for example, most cell phones: they generate a vibration from a varying voltage source.

Most energy harvesting systems based on piezoelectric materials aim to absorb energy from machine vibrations, pedestrian walks or wind turbulences, and can power loads ranging from tiny sensors from small vibrations to small communities through networks of large piezoelectric “towers” under wind turbulences. One of the most extended configurations consists of a piezoelectric beam or cantilever. Due to the elastic nature of the piezoelectric materials, they behave like damped oscillators which, in absence of a strong enough external forcing, tend to oscillate with small amplitude close to the resting position. In order to benefit higher energy oscillations, a typical approach consists of locating two magnets in inverse position as in Figure 1(b). If the magnets are strong enough with respect to the damping of the beam, in the absence of an external forcing, the resting vertical position (previously an attracting focus) becomes a saddle equilibrium and two new attracting foci appear pointing to each of the magnets.

The equations of motions for a generic (not necessarily piezoelectric) damped and forced beam with magnets as the one shown in Figure 1(a)

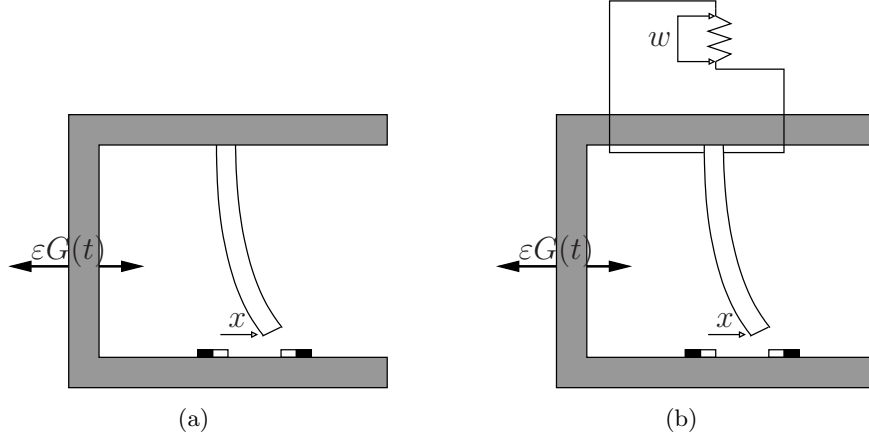


Figure 1: Generic elastic beam (a) and piezoelectric beam (b) subject to the influence of two magnets and a small periodic forcing.

were first derived in [23], which were shown to be a Duffing equation:

$$\ddot{x} + 2\zeta\dot{x} - \frac{1}{2}x(1 - x^2) = \varepsilon G(t),$$

where x is the dimensionless displacement of the lower end, ζ is the damping coefficient and $\varepsilon G(t)$ a small periodic forcing. When a piezoelectric beam is connected to a load in the upper end (as in Figure 1(b)), the load sees a certain voltage, w , whose time-derivative is proportional to the speed of lower displacement. From the point of view of the load, the piezoelectric beam acts as a capacitor. Hence, the voltage w follows the discharge law of a capacitor:

$$\dot{w} = -\lambda w - \kappa\dot{x},$$

where λ is a time constant associated with the capacitance of the piezoelectric beam and the resistance of the load, and $\kappa > 0$ is the electrical piezoelectric constant. However, in such a configuration, a mechanical auto-coupling effect occurs: the beam sees its own generated voltage w and the piezoelectric properties of the beam generates a strain opposite to the currently applied one. This not only has a dissipative effect, as it slows down the beam, but also increases the dimension of the system by one (see [9]), which becomes:

$$\begin{aligned} \ddot{x} + 2\zeta\dot{x} - \frac{1}{2}x(1 - x^2) - \chi w &= \varepsilon G(t) \\ \dot{w} &= -\lambda w - \kappa\dot{x}, \end{aligned}$$

where $\chi > 0$ is the mechanical piezoelectric constant.

The length of a piezoelectric beams or cantilevers plays a crucial role in the efficiency of the energy harvesting system, as it determines the frequency of the external forcing, $\varepsilon G(t)$, for which the device is “optimal”. Therefore, such devices need to be designed for particular frequencies. A big effort has been done from the design point of view to broaden this bandwidth. A common approach, introduced in [19], is to consider coupled oscillators of different lengths such that the device exhibits different voltage peaks at different frequencies. Other approaches consider different structural configurations ([11]) to achieve a similar improvement, or study the number of piezoelectric layers connected in different series-parallel configurations ([10]). However, mathematical studies of those models seem relegated to numerical simulations and bifurcation analysis [14, 25, 26]. As it was unveiled in [23], there exist very interesting dynamical phenomena already in the most simple case of a single beam under a periodic forcing, such as homoclinic tangles and horseshoes; also, in the absence of damping, KAM theory holds to show the existence of invariant curves. These, in the absence of damping, are boundaries in the state space and hence act as energy bounds. Therefore, assuming an external forcing of $O(\varepsilon)$, the amplitude of the oscillations of the beam cannot grow beyond this order hence restricting the amount of energy that can be absorbed from the source.

Even more interesting from the dynamical point of view is the higher dimensional case when considering two or more coupled damped oscillators. In this case, in the absence of damping, the dimension of KAM tori is not large enough to act as energy bounds and one may observe *Arnold diffusion*: existence of trajectories exhibiting $O(1)$ changes in their “energy” when the devices are driven by an arbitrarily small periodic forcing. Introduced in the celebrated paper of Arnold [1] researchers have recently achieved important rigorous results to prove the existence of such trajectories in general Hamiltonian systems [2, 22, 15]. The most paradigmatic applications of Arnold diffusion are associated with classical problems in celestial mechanics such as the *restricted three-body problem* and the Kirkwood gaps in the asteroids belt of the solar system [12], although it has also been proven in physical examples such as ABC magnetic fields [21].

The phenomenon of Arnold diffusion may be also relevant from a more applied point of view, for example related instabilities in mechanical structures can be very destructive, although it is desirable in energy harvesting systems and might help to improve their performance. Unfortunately, in real applications, one frequently finds obstacles such as dissipation or lack of regularity in order to apply the existent theory. For the latter, there has been already

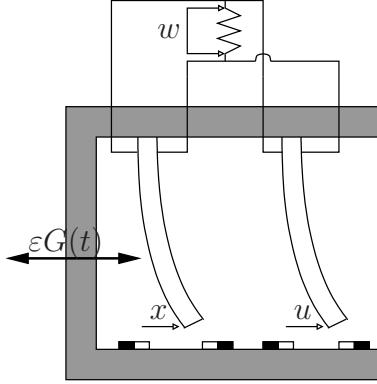


Figure 2: Energy harvester based on two piezoelectric beams.

theoretical contributions with applications to impacting mechanics [16].

In this work we present a first step on the study of Arnold diffusion in energy harvesting systems based on damped oscillators. In particular, we focus on a system based on the coupling of two piezoelectric beams as in Figure 2 and we perform a numerical study of the invariant objects and their connections. These play a crucial role in the known mechanisms for Arnold diffusion, which combine dynamics close to Normally Hyperbolic Manifolds (NHIM's) (*inner dynamics*) and *heteroclinic/homoclinic excursions* along the intersection of their stable and unstable manifolds. The study of the latter excursions was greatly facilitated after the introduction of the *scattering map* [7, 8]. In this article we have a less ambitious goal and we perform a first step in that direction: we perform a theoretical study of the existence and persistence of a NHIM, its numerical computation as well as its inner dynamics and its local stable and unstable manifolds by means of the so-called *parameterization method* [5, 18]. The study of homoclinic intersections and the scattering map is left for a future work. The main difficulty relies on the dimension of the system, which is 6-dimensional and the presence of dissipation in both the oscillators (through damping) and the coupling (inversed piezoelectric effect).

This work is organized as follows. In Section 2 we introduce the system in a perturbation setting: forcing and dissipation are included only in $O(\varepsilon)$ terms. We analyze its invariant objects for the unperturbed case and their persistence after introducing the perturbation. In Section 3 we present the theoretical setting necessary to apply a Newton-like method introduced

in [18] based on the parameterization method. In Section 4 we present the obtained numerical results, studying the inner dynamics for different configurations regarding the two type of dissipations (damping and piezoelectric coupling).

2 Invariant objects

2.1 Unperturbed system

Let x and u be the displacements of the both piezoelectric beams, and let $y = \dot{x}$ and $v = \dot{u}$. Calling w the (dimensionless) voltage on the resistor and adding time as a variable, from [20] we have that the equations of the model are

$$\begin{aligned}\dot{x} &= y \\ \dot{y} &= -2\zeta y + \frac{1}{2}x(1 - x^2) + \chi w + \varepsilon G(s) \\ \dot{u} &= v \\ \dot{v} &= -2\zeta v + \frac{1}{2}\beta u(1 - u^2) + \chi w + \varepsilon G(s) \\ \dot{w} &= -\lambda w - \kappa(y + v) \\ \dot{s} &= 1,\end{aligned}$$

where $G(s)$ is a T -periodic forcing, λ is a time constant of the electrical circuit and χ and κ are the dimensionless piezoelectric couplings in the mechanical and electrical equations, respectively. The parameter $\beta \simeq 1$ compensates possible mistuning of the parameters.

Let us now assume that the damping (ζ), the piezoelectric couplings (χ and κ) and the amplitude of the external forcing are small. We can then introduce a perturbation parameter, $\varepsilon > 0$, and, after performing the parametrizations

$$\zeta = \varepsilon \tilde{\zeta}, \quad \chi = \varepsilon \tilde{\chi} \tag{1}$$

we can write the system as

$$\dot{\tilde{z}} = g_0(\tilde{z}) + \varepsilon g_1(\tilde{z}) \tag{2}$$

where $\tilde{z} = (x, y, u, v, w, s) \in \mathbb{R}^5 \times \mathbb{T}_T = \mathbb{R}^5 \times \mathbb{R}/T\mathbb{Z}$,

$$g_0(\tilde{z}) = \begin{pmatrix} y \\ \frac{1}{2}x(1-x^2) \\ v \\ \frac{1}{2}\beta u(1-u^2) \\ -\lambda w - k(y+v) \\ 1 \end{pmatrix}$$

and

$$g_1(\tilde{z}) = \begin{pmatrix} 0 \\ -2\tilde{\zeta}y + \tilde{\chi}w + G(s) \\ 0 \\ -2\tilde{\zeta}v + \tilde{\chi}w + G(s) \\ 0 \\ 0 \end{pmatrix} \quad (3)$$

The unperturbed system,

$$\dot{\tilde{z}} = g_0(\tilde{z}) \quad (4)$$

consists of two uncoupled systems, one for each beam in \mathbb{R}^2 , the equation for \dot{w} describing the piezoelectric coupling and the time evolution $\dot{s} = 1$. Each of the systems describing the motion of the beams ([23]) is Hamiltonian,

$$\begin{aligned} \mathcal{X}(x, y) &= \frac{y^2}{2} - \frac{1}{4}x^2 \left(1 - \frac{x^2}{2}\right) \\ \mathcal{U}(u, v) &= \frac{v^2}{2} - \frac{1}{4}u^2\beta \left(1 - \frac{u^2}{2}\right). \end{aligned}$$

The phase portrait for each of oscillator is shown in Figure 3 and consists of a figure of eight. It posses three equilibrium points:

$$\begin{aligned} Q^\pm &= (\pm 1, 0) \\ Q_0 &= (0, 0). \end{aligned}$$

The origin Q_0 is a saddle point with two eight-figured homoclinic loops,

$$\gamma^\pm := \mathcal{W}^s(Q_0) \cap \mathcal{W}^u(Q_0) = \mathcal{W}^s(Q_0) = \mathcal{W}^u(Q_0), \quad (5)$$

such that

$$\gamma^+ \cup \{Q_0\} \cup \gamma^- = \{(x, y) \in \mathbb{R}^2, \mathcal{X}(x, y) = 0\}.$$

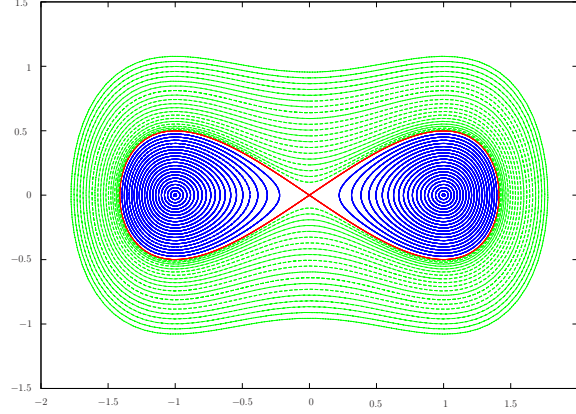


Figure 3: Phase portrait of each beam in absence of forcing and dissipation.

We consider parametrizations

$$\gamma^\pm = \{\sigma^\pm(t), t \in \mathbb{R}\} \quad (6)$$

satisfying

$$\begin{aligned} \lim_{t \rightarrow \pm\infty} \sigma^\pm(t) &= Q_0 \\ \sigma^\pm(0) &= (0, \pm\sqrt{2}). \end{aligned}$$

Each homoclinic loop γ^\pm surrounds the equilibrium point Q^\pm . The points Q^\pm are elliptic points, and the region bounded by the homoclinic loops are covered by periodic orbits.

For our construction, we will be interested in the periodic orbits located outside the homoclinic loops for system \mathcal{U}

$$\mathcal{P}_c = \{(u, v) \in \mathbb{R}^2, |\mathcal{U}(u, v) = c\}, \quad (7)$$

with $c > 0$, while system \mathcal{X} remains close to the hyperbolic point Q_0 . Similar invariant objects to the ones below can be obtained when focusing on the two type of periodic orbits inside the homoclinic loops and surrounding each of the elliptic points Q^\pm .

The periods of the periodic orbits Λ_c can be computed as follows. Consider the periodic orbit with initial condition $(0, v_0)$, with level of energy

$$c = \frac{v_0^2}{2},$$

which crosses the u axis at the point

$$(u_1, 0) = \left(\sqrt{1 + \sqrt{1 + \frac{8c}{\beta}}}, 0 \right).$$

Using the symmetries of the system and its Hamiltonian structure, we obtain that the period of a periodic orbit \mathcal{P}_c , with $c = \frac{v_0^2}{2}$, becomes

$$\begin{aligned} \alpha_c &:= 4 \int_0^{u_1} \frac{1}{\dot{u}} du \\ &= 4 \int_0^{u_1} \frac{1}{\sqrt{2c + \beta \frac{u^2}{2} \left(1 - \frac{u^2}{2}\right)}} du. \end{aligned} \quad (8)$$

We now focus on the reduced dynamics given by these periodic orbits for system \mathcal{U} while systems \mathcal{X} remains at its equilibrium point Q_0 . Provided that each of these periodic orbits is contained in the energy level given by $\mathcal{U}(u, v) = c$, it will be more natural to parametrize them by c and an angle, θ . Hence we will consider “action angle”-like parameters $(\theta, c) \in \mathbb{T} \times \mathbb{R}$ to parametrize periodic orbits \mathcal{P}_c as follows. Letting $\varphi_{\mathcal{U}}(t; u_0, v_0)$ be the flow associated with system \mathcal{U} such that $\varphi_{\mathcal{U}}(0; u_0, v_0) = (u_0, v_0)$, we consider

$$\begin{aligned} p : \quad \mathbb{T} \times \mathbb{R} &\longrightarrow \mathbb{R}^2 \\ (\theta, c) &\longmapsto \varphi_{\mathcal{U}}(\theta \alpha_c; 0, \sqrt{2c}). \end{aligned} \quad (9)$$

Note that this induces the dynamics

$$\begin{aligned} \dot{\theta} &= \frac{1}{\alpha_c} \\ \dot{c} &= 0. \end{aligned}$$

When $(x, y) = Q_0$, provided that $\lambda > 0$, the variable w is attracted to a certain object given by the dynamics of v . Writing

$$v^p(t; u_0, v_0) = \Pi_v(\varphi_{\mathcal{U}}(t; u_0, v_0)), \quad (10)$$

the dynamics of w restricted to $(x, y) = Q_0 = (0, 0)$ are given by

$$\dot{w} = -\lambda w - k v^p(t). \quad (11)$$

Provided that for $k = 0$ Equation (11) is linear and that $v_p(t)$ is α_c -periodic, the α_c -time return map associated with system (11) possesses a fixed point for any value of k and, hence, system (11) possesses an α_c -periodic orbit:

$$w^p(t + \alpha_c) = w^p(t),$$

which is attracting.

Let us now compute the initial condition for such periodic orbit. Note that, although system (11) is not autonomous, we can assume that initial conditions are given for $t = 0$, since Equation (11) has to be integrated together with the equations for \dot{u} and \dot{v} , forming an autonomous system. Therefore, the general solution of (11) becomes

$$w(t; w_0) = e^{-\lambda t} \left(\int_0^t -kv_p(s)e^{\lambda s} ds + w_0 \right),$$

from where, imposing $w(\alpha_c; w_0) = w_0$, we get that the initial condition for a periodic orbit is

$$w_0^p = \frac{e^{-\lambda \alpha_c}}{1 - e^{-\lambda \alpha_c}} \int_0^{\alpha_c} -kv^p(s)e^{\lambda s} ds.$$

Hence, given (u_0, v_0) , the attracting periodic orbit of w becomes

$$w^p(t) = e^{-\lambda t} \left(\int_0^t -kv^p(s)e^{\lambda s} ds + \frac{e^{-\lambda \alpha_c}}{1 - e^{-\lambda \alpha_c}} \int_0^{\alpha_c} -kv^p(s)e^{\lambda s} ds \right).$$

Note that w_0^p depends on u_0 and v_0 through the periodic orbit (10). To emphasize it, we will write $w_0^p(u_0, v_0)$. Note that $w_0^p(u_0, v_0)$ is indeed a parametrization of the whole periodic orbit $w^p(t)$, just by keeping $t = 0$ and varying u, v along the periodic orbit \mathcal{P}_c . Hence we have obtained the 3-dimensional invariant manifold

$$\tilde{\mathcal{K}} = Q_0 \times \left(\bigcup_{c_1 \leq c \leq c_2} \left\{ (u, v, w) \mid \mathcal{U}(u, v) = c, w = w_0^p(u, v) \right\} \right) \times \mathbb{T}_T \subset \mathbb{R}^5 \times \mathbb{T}_T.$$

Recalling that (u_0, v_0) can be parametrized by $p(\theta, c)$, w_0^p can be as well parametrized by θ and c , $w^p(p(\theta, c))$. This induces a parametrization for $\tilde{\mathcal{K}}$

$$\tilde{K}_0 : \mathbb{T} \times \mathbb{R} \times \mathbb{T}_T \longrightarrow \mathbb{R}^5 \times \mathbb{T}_T, \quad (12)$$

given by

$$\tilde{K}_0(\theta, c, s) = \begin{pmatrix} 0 \\ 0 \\ p(\theta, c) \\ w_0^p(p(\theta, c)) \\ s \end{pmatrix} \quad (13)$$

and hence

$$\tilde{\mathcal{K}} = \tilde{K}_0(\mathbb{T}, [c_1, c_2], \mathbb{T}_T),$$

The invariant manifold $\tilde{\mathcal{K}}$ is foliated by 2-dimensional invariant tori contained at energy level c :

$$\tilde{\mathcal{K}} = Q_0 \times \bigcup_{c_1 \leq c \leq c_2} \tilde{\mathcal{K}}_c.$$

Each of these tori is homeomorphic to $\mathbb{T} \times \mathbb{T}_T$,

$$\tilde{\mathcal{K}}_c \simeq \mathbb{T} \times \mathbb{T}_T,$$

as it can be parametrized by (θ, s) :

$$\tilde{\mathcal{K}}_c = \tilde{K}_0^c(\mathbb{T}, \mathbb{T}_T),$$

where

$$\begin{aligned} \tilde{K}_0^c : \mathbb{T} \times \mathbb{T}_T &\longrightarrow \mathbb{R}^3 \times \mathbb{T}_T \\ (\theta, s) &\longmapsto \Pi_{u,v,w,s} \left(\tilde{K}_0(\theta, c, s) \right). \end{aligned} \quad (14)$$

When c is such that T and α_c are congruent, then $\tilde{\mathcal{K}}_c$ is filled by periodic orbits: each point is a periodic point of the $2\pi/\omega$ -time return map. However, when T and α_c are incommensurable, $\tilde{\mathcal{K}}_c$ is densely filled by any solution with initial conditions at $\tilde{\mathcal{K}}_c$. Note that this implies that, for any point in $\tilde{\mathcal{K}}$, one obtains bounded dynamics both for $t \rightarrow \infty$ and $t \rightarrow -\infty$.

We now show that $\tilde{\mathcal{K}}$ is a normally hyperbolic invariant manifold (NHIM), by showing that it has stable and unstable manifolds with exponential convergence.

The hyperbolicity is inherited from the hyperbolic point Q_0 . We consider (x, y) coordinates at one of the homoclinic loops of Q_0 parametrized by τ :

$$\sigma(\tau) \in \gamma, \quad (15)$$

where $\sigma(\tau)$ can be either $\sigma^+(\tau)$ or $\sigma^-(\tau)$ (similarly for γ). We also fix parameters θ, c, s leading to a point

$$\tilde{K}_0^c(\theta, s) = (u, v, w, s) \in \tilde{\mathcal{K}}_c. \quad (16)$$

Letting $\varphi_{\mathcal{X}}(t; x, y)$ be the flow associated with the Hamiltonian \mathcal{X} , we call

$$y^h(t; \tau) = \Pi_y(\varphi_{\mathcal{X}}(t; \sigma(\tau))).$$

We may omit explicit dependence of y^h on τ .

When restricted to the conditions (15)-(16), the variable w evolves following the equation

$$\dot{w} = -\lambda w - k(y^h(t) + v^p(t)), \quad (17)$$

which has the general solution

$$w(t) = e^{-\lambda t} \left(w_0 - \int_0^t k \left(y^h(s) + v^p(s) \right) e^{\lambda s} ds \right). \quad (18)$$

Then, the stable and unstable manifolds $\mathcal{W}^s(\tilde{K})$ and $\mathcal{W}^u(\tilde{K})$ will be given by (15)-(16) and solutions of (18) satisfying

$$\lim_{t \rightarrow \infty} |w^s(t) - w^p(t)| \rightarrow 0$$

and

$$\lim_{t \rightarrow -\infty} |w^u(t) - w^p(t)| \rightarrow 0.$$

In order to find $w^u(0)$ and $w^s(0)$, let us define

$$z(t) = w(t) - w^p(t) = e^{-\lambda t} \left(z_0 - \int_0^t k y^h(s) e^{\lambda s} ds \right),$$

where

$$z_0 = w(0) - w^p(0). \quad (19)$$

Due to the hyperbolicity of Q_0 , we know that there exist positive constants $\tilde{\lambda}$, M and δ such that

$$|y^h(t) - 0| < M e^{-\tilde{\lambda}|t|}, \quad |t| > \delta$$

Hence, we get that

$$\begin{aligned} \lim_{t \rightarrow +\infty} |z(t)| &= \lim_{t \rightarrow +\infty} \left(e^{-\lambda t} z_0 - \int_0^t k y^h(s) e^{\lambda(s-t)} ds \right) \\ &< \lim_{t \rightarrow +\infty} \int_0^t k e^{-\tilde{\lambda}s + \lambda(s-t)} ds = 0, \end{aligned}$$

for any $z_0 \in \mathbb{R}$, and all initial conditions for w are attracted to the periodic orbit $w^p(t)$.

However, the limit for $t \rightarrow -\infty$ diverges unless we choose

$$z_0 = - \int_{-\infty}^0 k e^{\lambda s} y^h(s) ds.$$

In this case, we get

$$\begin{aligned}
\lim_{t \rightarrow -\infty} |z(t)| &= \lim_{t \rightarrow -\infty} \left| e^{-\lambda t} \left(\int_{-\infty}^0 k e^{\lambda s} y^h(s) ds + \int_0^t k e^{\lambda s} y^h(s) ds \right) \right| \\
&= \lim_{t \rightarrow -\infty} \left| e^{-\lambda t} \int_{-\infty}^t k e^{\lambda s} y^h(s) ds \right| \\
&< \lim_{t \rightarrow -\infty} \left| e^{-\lambda t} \int_{-\infty}^t k M e^{(\lambda + \tilde{\lambda})s} ds \right| \\
&= \lim_{t \rightarrow -\infty} \frac{k M e^{\tilde{\lambda} t}}{\lambda + \tilde{\lambda}} = 0.
\end{aligned}$$

Summarizing, we have proven the following result.

Lemma 1. *System (4) possesses a foliated normally hyperbolic manifold*

$$\tilde{\mathcal{K}} = Q_0 \times \bigcup_{c_1 \leq c \leq c_2} \tilde{\mathcal{K}}_c$$

with

$$\begin{aligned}
\tilde{\mathcal{K}}_c &= \left\{ (u, v, w, s) \in \mathcal{P}_c \times \mathbb{R} \times \mathbb{T}_T, |w = w_0^p(u, v) \right\} \\
\mathcal{P}_c &= \left\{ (u, v) \in \mathbb{R}^2, |\mathcal{U}(u, v) = c \right\} \\
w_0^p(u, v) &= \frac{e^{-\lambda \alpha_c}}{1 - e^{-\lambda \alpha_c}} \int_0^{\alpha_c} -k v^p(s; u, v) e^{\lambda s} ds \\
v^p(s; u, v) &= \Pi_v(\varphi_{\mathcal{U}}(s; u, v)).
\end{aligned} \tag{20}$$

The manifold $\tilde{\mathcal{K}}$ is normally hyperbolic, has a 5-dimensional stable manifold

$$\mathcal{W}^s(\tilde{\mathcal{K}}) = \mathcal{W}^s(Q_0) \times \bigcup_{c \in [c_1, c_2]} \mathcal{P}_c \times \mathbb{R} \times \mathbb{T}_T$$

and a 4-dimensional unstable manifold given by the union of two homoclinic loops,

$$\mathcal{W}^u(\tilde{\mathcal{K}}) = \tilde{\Gamma}^+ \cup \tilde{\Gamma}^- \subset \mathcal{W}^s(\tilde{\mathcal{K}}),$$

where

$$\begin{aligned}\tilde{\Gamma}^+ &= \bigcup_{c_1 \leq c \leq c_2} \left\{ (x, y, u, v, w, s) \in \gamma^+ \times \mathcal{P}_c \times \mathbb{R} \times \mathbb{T}_T, \right. \\ &\quad \left. w = w_0^u(x, y, u, v) \right\} \\ \tilde{\Gamma}^- &= \bigcup_{c_1 \leq c \leq c_2} \left\{ (x, y, u, v, w, s) \in \gamma^- \times \mathcal{P}_c \times \mathbb{R} \times \mathbb{T}_T, \right. \\ &\quad \left. w = w_0^u(x, y, u, v) \right\}\end{aligned}$$

and

$$\begin{aligned}w_0^u(x, y, u, v) &= - \int_{-\infty}^0 k e^{\lambda s} y^h(s; x, y) ds + w_0^p(u, v) \\ y^h(s; x, y) &= \Pi_y(\varphi_{\mathcal{X}}(s; x, y)) \\ (x, y) &\in \gamma^+ \cup \gamma^-.\end{aligned}\tag{21}$$

There exist parametrizations such that these manifolds can be written as

$$\begin{aligned}\mathcal{P}_c &= p(\mathbb{T}, c) \\ \tilde{\mathcal{K}}_c &= \tilde{K}_0^c(\mathbb{T}, \mathbb{T}_T) \\ \tilde{\mathcal{K}} &= \tilde{K}_0(\mathbb{T}, [c_1, c_2], \mathbb{T}_T) \\ \mathcal{W}^s(\tilde{\mathcal{K}}) &= \tilde{W}_0^{s,+}(\mathbb{T}, [c_1, c_2], \mathbb{T}_T, \mathbb{R}^2) \\ &\quad \cup \tilde{W}_0^{s,-}(\mathbb{T}, [c_1, c_2], \mathbb{T}_T, \mathbb{R}^2) \\ \mathcal{W}^u(\tilde{\mathcal{K}}) &= \tilde{W}_0^{u,+}(\mathbb{T}, [c_1, c_2], \mathbb{T}_T, \mathbb{R}) \\ &\quad \cup \tilde{W}_0^{u,-}(\mathbb{T}, [c_1, c_2], \mathbb{T}_T, \mathbb{R})\end{aligned}$$

where

$$\begin{aligned}p : \quad \mathbb{T} \times (0, \infty) &\longrightarrow \mathbb{R}^2 \\ (\theta, c) &\longmapsto \varphi_{\mathcal{U}}(\theta \alpha_c; 0, \sqrt{2c}) \\ \tilde{K}_0^c : \quad \mathbb{T} \times \mathbb{T}_T &\longrightarrow \mathbb{R}^3 \times \mathbb{T}_T \\ (\theta, s) &\longmapsto (p(\theta, c), w_0^p(p(\theta, c)), s) \\ \tilde{K}_0 : \quad \mathbb{T} \times \mathbb{R} \times \mathbb{T}_T &\longrightarrow \mathbb{R}^5 \times \mathbb{T}_T \\ (\theta, c, s) &\longmapsto (0, 0, \tilde{K}_0^c(\theta, s)) \\ \tilde{W}_0^{s,\pm} : \quad \mathbb{T} \times [c_1, c_2] \times \mathbb{T}_T \times \mathbb{R}^2 &\longrightarrow \mathbb{R}^5 \times \mathbb{T}_T \\ (\theta, c, s, \tau, r) &\longmapsto (\sigma^\pm(\tau), p(\theta, c), r, s) \\ \tilde{W}_0^{u,\pm} : \quad \mathbb{T} \times [c_1, c_2] \times \mathbb{T}_T \times \mathbb{R} &\longrightarrow \mathbb{R}^5 \times \mathbb{T}_T \\ (\theta, c, s, \tau) &\longmapsto (\sigma^\pm(\tau), p(\theta, c), w_0^u(\sigma^\pm(\tau), p(\theta, c)), s)\end{aligned}$$

2.2 Persistence of manifolds

For $\varepsilon > 0$ theory of normally hyperbolic invariant manifolds (see [13]) guarantees that (locally) there exists $\tilde{\mathcal{K}}_\varepsilon$ ε -close to $\tilde{\mathcal{K}}$, with $\tilde{\mathcal{K}}_0 = \tilde{\mathcal{K}}$. However, in the case of considering only the perturbation given by the external forcing ($\varepsilon > 0$ and $\zeta = \tilde{\chi} = 0$), the perturbation becomes Hamiltonian. Hence, as the system remains uncoupled, the inner dynamics is symplectic and KAM Theorem ([6]) holds. This guarantees us that, those periodic orbits whose periods are, modulo T , away enough from rational numbers, persist as invariant tori. Hence, in the Hamiltonian case, this manifold $\tilde{\mathcal{K}}_\varepsilon$ is a manifold with boundaries and hence it becomes a globally unique manifold. Indeed we will assume that the curves $c = c_1$ and $c = c_2$ parametrize two invariant tori consisting of the lower and upper boundaries of the manifold.

When the perturbation includes dissipative terms ($\tilde{\zeta} > 0$ and/or $\tilde{\chi} > 0$), the existence of these boundaries is not guaranteed. Indeed, as it will be shown in Section 4, the inner dynamics contains a global attractor in either case. As a consequence of that, KAM tori do not necessarily persist and $\tilde{\mathcal{K}}_\varepsilon$ becomes a manifold without boundaries. Therefore, theory for normally hyperbolic manifold can only guaranty its local uniqueness.

Hence we have parameterizations

$$\tilde{K}_\varepsilon : \mathbb{T} \times [c_1, c_2] \times \mathbb{T}_T \longrightarrow \mathbb{R}^5 \times \mathbb{T}_T \quad (22)$$

$$\tilde{W}_\varepsilon^{s,\pm} : \mathbb{T} \times [c_1, c_2] \times \mathbb{T}_T \times \mathbb{R}^2 \longrightarrow \mathbb{R}^5 \times \mathbb{T}_T \quad (23)$$

$$\tilde{W}_\varepsilon^{u,\pm} : \mathbb{T} \times [c_1, c_2] \times \mathbb{T}_T \times \mathbb{R} \longrightarrow \mathbb{R}^5 \times \mathbb{T}_T \quad (24)$$

such that

$$\begin{aligned} \tilde{\mathcal{K}}_\varepsilon &= \tilde{K}_\varepsilon(\mathbb{T}, [c_1, c_2], \mathbb{T}_T) \\ \mathcal{W}^s(\tilde{\mathcal{K}}_\varepsilon) &= \tilde{W}_\varepsilon^{s,+}(\mathbb{T}, [c_1, c_2], \mathbb{T}_T, \mathbb{R}^2) \\ &\quad \cup \tilde{W}_\varepsilon^{s,-}(\mathbb{T}, [c_1, c_2], \mathbb{T}_T, \mathbb{R}^2) \\ \mathcal{W}^u(\tilde{\mathcal{K}}_\varepsilon) &= \tilde{W}_\varepsilon^{u,+}(\mathbb{T}, [c_1, c_2], \mathbb{T}_T, \mathbb{R}) \\ &\quad \cup \tilde{W}_\varepsilon^{u,-}(\mathbb{T}, [c_1, c_2], \mathbb{T}_T, \mathbb{R}). \end{aligned}$$

These parameterizations, together with the dynamics of the system when restricted to $\tilde{\mathcal{K}}_\varepsilon$ and linear approximations of the manifolds $\mathcal{W}_\varepsilon^s(\tilde{\mathcal{K}}_\varepsilon)$ and $\mathcal{W}_\varepsilon^u(\tilde{\mathcal{K}}_\varepsilon)$ will be numerically computed in Section 3.

3 Numerical framework for the parameterization method

In this section we numerically compute the perturbed Normally Hyperbolic Manifold $\tilde{\mathcal{K}}_\varepsilon$ by means of the so-called parameterization method, introduced in [3, 4, 5].

The parameterization method is stated easier when formulated for maps; hence, it will be more convenient to write the full system (2) as discrete system. The most natural map to consider is of course the stroboscopic map, due to the periodicity of the system. However, due to the foliated nature of the unperturbed manifold $\tilde{\mathcal{K}}_0$, instead of using the original variables, we will consider from now on the induced map in the manifolds introduced in Section 2.1:

$$\begin{aligned} F_\varepsilon : \quad \mathbb{T} \times (0, \infty) \times \mathbb{R}^3 &\longrightarrow \mathbb{T} \times (0, \infty) \times \mathbb{R}^3 \\ (\theta, c, x, y, w) &\longmapsto \tilde{p} \circ \mathfrak{s}_\varepsilon \circ \tilde{p}^{-1}(\theta, c, x, y, w), \end{aligned} \quad (25)$$

where \tilde{p} is the change of variables

$$\tilde{p}(\theta, c, x, y, w) = (x, y, p(\theta, c), w) = (x, y, \varphi_{\mathcal{U}}(\theta\alpha_c; 0, \sqrt{2c}), w)$$

and \mathfrak{s}_ε is the stroboscopic map

$$\begin{aligned} \mathfrak{s}_\varepsilon : \quad \Sigma_{s_0} &\longrightarrow \Sigma_{s_0} \\ (x, y, u, v, w) &\longmapsto \tilde{\phi}_\varepsilon(s_0 + 2\pi/\omega; x, y, u, v, w, s). \end{aligned}$$

As shown in Section 2.2, the time continuous perturbed system possesses a Normally Hyperbolic Manifold $\tilde{\mathcal{K}}_\varepsilon$ parameterized by \tilde{K}_ε (22). Hence, the discrete time system also possesses a Normally Hyperbolic Manifold (a cylinder), \mathcal{K}_ε , given by a parameterization

$$K_\varepsilon : \mathbb{T} \times [c_1, c_2] \longrightarrow \mathbb{T} \times (0, \infty) \times \mathbb{R}^3, \quad (26)$$

such that

$$\mathcal{K}_\varepsilon = K_\varepsilon(\mathbb{T} \times [c_1, c_2]).$$

The map F_ε restricted to K_ε induces inner dynamics in \mathcal{K}_ε . Recalling that, as assumed in Section 2.2 $c = c_1$ and $c = c_2$ parameterize lower and upper boundaries of \mathcal{K}_ε , respectively, given by two invariant curves, the inner dynamics are given by a map

$$f_\varepsilon : \mathbb{T} \times [c_1, c_2] \longrightarrow \mathbb{T} \times [c_1, c_2].$$

The parameterization methods consists of finding K_ε and f_ε such that the diagram

$$\begin{array}{ccc} \mathbb{T} \times [c_1, c_2] & \xrightarrow{K_\varepsilon} & \mathbb{T} \times (0, \infty) \times \mathbb{R}^3 \\ \downarrow f_\varepsilon & & \downarrow F_\varepsilon \\ \mathbb{T} \times [c_1, c_2] & \xrightarrow{K_\varepsilon} & \mathbb{T} \times (0, \infty) \times \mathbb{R}^3 \end{array}$$

commutes. Note that, although we don't have an explicit expression, we can consider that the map F_ε is given, provided that we can numerically compute the stroboscopic map \mathfrak{s} . Hence, we need to solve the cohomological

$$F_\varepsilon \circ K_\varepsilon - K_\varepsilon \circ f_\varepsilon = 0 \quad (27)$$

for the unknowns f_ε and K_ε .

This can be done in many different ways, mainly depending on whether the inner dynamics, f_ε , is known (or imposed when computing invariant curves for a particular frequency) or not. In our case, the unknowns are both f_ε and K_ε , and we follow the method described in [18] (Chapter 5). It consists of taken advantage of the hyperbolicity of \mathcal{K}_ε to perform a Newton-like method to compute functions f_ε and K_ε . In practice, given a discretization of the reference manifold $\mathbb{T}_T \times [c_1, c_2]$, this means that we want to compute the coefficients for approximations (splines, Fourier series or Lagrangian polynomials) of f_ε and K_ε . We first review the method described in [18] adapted to our case.

3.1 A Newton-like method

Assume that, for a certain $\varepsilon > 0$, we have a good enough approximations of K_ε and f_ε . As usual in Newton-like methods, in order to provide new approximations, we will require as well initial approximations of the dynamics at the tangent bundles; that is, approximations of the solutions to the cohomological equation

$$DF_\varepsilon(K_\varepsilon(\theta, c)) - DK_\varepsilon(f_\varepsilon(\theta, c)) = 0. \quad (28)$$

Note that Equation (28) manifests the invariance of the tangent bundle TK_ε under DF_ε , leading to inner dynamics at TK_ε given by Df_ε . However, DF_ε is a map onto the tangent space $T(\mathbb{T} \times \mathbb{R} \times \mathbb{R}^3)$. The latter can be generated by two vectors in TK_ε and three in the normal bundle NK_ε , $T(\mathbb{T} \times \mathbb{R} \times \mathbb{R}^3) = TK_\varepsilon \times NK_\varepsilon$. Provided that \mathcal{K}_ε is normally hyperbolic, the normal space NK_ε can be generated by two vectors tangent to $\mathcal{W}^s(\mathcal{K}_\varepsilon)$

and a third one tangent to $\mathcal{W}^u(\mathcal{K})$. It will be hence useful to consider the adapted frame around \mathcal{K}_ε

$$P_\varepsilon(\theta, c) = (L_\varepsilon(\theta, c) \ N_\varepsilon(\theta, c)),$$

given by the juxtaposition of the matrices L and N , where

$$L_\varepsilon(\theta, c) = DK_\varepsilon(\theta, c)$$

is a 5×2 matrix and $N(\theta, c)$ is 5×3 given by the three columns of DF_ε generating the normal bundle $N\mathcal{K}_\varepsilon$.

The matrix P_ε can be seen as a change of basis such that the skew product

$$(f_\varepsilon, \Lambda_\varepsilon) : \mathbb{T} \times [c_1, c_2] \times \mathbb{R}^5 \longrightarrow \mathbb{T} \times [c_1, c_2] \times \mathbb{R}^5,$$

with

$$\Lambda_\varepsilon = P_\varepsilon(f(\theta, c))^{-1} DF_\varepsilon(K_\varepsilon(\theta, c)) P_\varepsilon(\theta, c),$$

becomes of the form

$$\Lambda_\varepsilon = \begin{pmatrix} \Lambda_\varepsilon^L & 0 & 0 & 0 \\ 0 & 0 & \Lambda_\varepsilon^S & 0 \\ 0 & 0 & 0 & 0 \\ 0 & 0 & 0 & 0 \end{pmatrix} \Lambda_\varepsilon^U.$$

Note that

$$\Lambda_\varepsilon^L = Df_\varepsilon.$$

The Newton-like method consists of two steps. Given approximations of K_ε (and hence $L_\varepsilon = DK_\varepsilon$), f_ε (and hence $\Lambda_\varepsilon^L = Df_\varepsilon$), Λ_ε^S and Λ_ε^N , in the first step, one computes new corrected versions of K_ε and f_ε (and hence L_ε and Λ_ε^L). In the second step, one corrects the normal bundle N and its linearized dynamics Λ_ε^N .

3.1.1 First step: correction of the manifold and the inner dynamics

Following [18], we consider corrections of the form

$$\begin{aligned} \bar{f}_\varepsilon &= f_\varepsilon + \Delta f_\varepsilon \\ \bar{K}_\varepsilon &= K_\varepsilon + \Delta K_\varepsilon, \end{aligned}$$

with

$$\Delta K_\varepsilon = P_\varepsilon(\theta, c)\zeta(\theta, c).$$

We want to compute $\zeta(\theta, c)$ and $\Delta f_\varepsilon(\theta, c)$.

The corrections of the manifold, $\zeta(\theta, c)$, can be split in tangent, stable and unstable directions:

$$\zeta(\theta, c) = \begin{pmatrix} \zeta^L(\theta, c) \\ \zeta^S(\theta, c) \\ \zeta^U(\theta, c) \end{pmatrix} \in \mathbb{R}^2 \times \mathbb{R}^2 \times \mathbb{R}.$$

Let $E(\theta, c)$ be the error at Equation (27) at the current value f_ε and K_ε ,

$$E(\theta, c) = F_\varepsilon(K_\varepsilon(\theta, c)) - K_\varepsilon(f_\varepsilon(\theta, c)).$$

Let

$$\eta(\theta, c) = -(P(f(\theta, c)))^{-1} E(\theta, c),$$

which, again, we split in tangent, stable and unstable directions

$$\eta(\theta, c) = \begin{pmatrix} \eta^L(\theta, c) \\ \eta^S(\theta, c) \\ \eta^U(\theta, c) \end{pmatrix}.$$

Then, assuming that

$$\zeta^L(\theta, c) = \begin{pmatrix} 0 \\ 0 \end{pmatrix},$$

that is, the manifold $K_\varepsilon(\mathbb{T}, [c_1, c_2])$ is only corrected in the normal directions, Δf_ε becomes

$$\Delta f_\varepsilon(\theta, c) = -\eta^L(\theta, c)$$

(see [18] for more details).

Regarding ΔK_ε , by expanding Equation (27), one gets that ζ^S and ζ^U satisfy the equations

$$\eta^S(\theta, c) = \Lambda_\varepsilon^S(\theta, c)\zeta^S(\theta, c) - \zeta^S(\theta, c) \quad (29)$$

$$\eta^U(\theta, c) = \Lambda_\varepsilon^U(\theta, c)\zeta^U(\theta, c) - \zeta^U(\theta, c). \quad (30)$$

Due to hyperbolicity, $\Lambda_\varepsilon^U > 1$ and the eigenvalues of Λ_ε^S are real, positive and inside the unite circle. Hence, Equations (29)-(30) can be solved by iterating the systems

$$\begin{aligned} \zeta^S(\theta, c) &= \Lambda_\varepsilon^S(f^{-1}(\theta, c))\zeta^S(f^{-1}(\theta, c)) - \eta^S(f^{-1}(\theta, c)) \\ \zeta^U(\theta, c) &= \frac{\zeta^U(f(\theta, c)) + \eta^U(\theta, c)}{\Lambda_\varepsilon^U(\theta, c)}. \end{aligned}$$

3.1.2 Second step: normal bundle correction

Once we have new corrected versions of the inner dynamics $f_\varepsilon(\theta, c)$ (and consequently $\Lambda_\varepsilon^L(\theta, c)$) and the parametrization $K_\varepsilon(\theta, c)$ (and consequently $L(\theta, c)$), the second step consists of computing new approximations for Λ_ε^S , Λ_ε^U and $N_\varepsilon(\theta, c)$. As in [18], we consider approximations of the form

$$\begin{aligned}\bar{N}_\varepsilon(\theta, c) &= N_\varepsilon(\theta, c) + \Delta N(\theta, c) \\ \bar{\Lambda}_\varepsilon^S(\theta, c) &= \Lambda_\varepsilon^S(\theta, c) + \Delta \Lambda^S(\theta, c) \\ \bar{\Lambda}_\varepsilon^U(\theta, c) &= \Lambda_\varepsilon^U(\theta, c) + \Delta \Lambda^U(\theta, c),\end{aligned}$$

with

$$\Delta N(\theta, c) = P_\varepsilon(\theta, c) Q^N(\theta, c).$$

Assuming that the corrections of the linearized stable and unstable bundles are done in the complementary directions, one gets that $Q^N(\theta, c)$ is of the form

$$Q^N(\theta, c) = \begin{pmatrix} Q^{LS}(\theta, c) & Q^{LU}(\theta, c) \\ 0 & 0 & Q^{SU}(\theta, c) \\ 0 & 0 & 0 \\ Q^{US}(\theta, c) & 0 \end{pmatrix}.$$

Let us write the current error in the cohomological equation at the tangent bundle (Equation (28)) as

$$\begin{aligned}E_{\text{red}}^N(\theta, c) &= P_\varepsilon(\theta, c)^{-1} D F_\varepsilon(K_\varepsilon(\theta, c)) N_\varepsilon(\theta, c) - \\ &- \begin{pmatrix} 0 & 0 & 0 \\ 0 & 0 & 0 \\ \Lambda_\varepsilon^S(\theta, c) & 0 & 0 \\ 0 & 0 & \Lambda_\varepsilon^U(\theta, c) \end{pmatrix} = \begin{pmatrix} E_{\text{red}}^{LS}(\theta, c) & E_{\text{red}}^{LU}(\theta, c) \\ E_{\text{red}}^{SS}(\theta, c) & E_{\text{red}}^{SU}(\theta, c) \\ E_{\text{red}}^{US}(\theta, c) & E_{\text{red}}^{UU}(\theta, c) \end{pmatrix}\end{aligned}$$

On one hand, the corrections of the adapted frame in the normal directions become

$$\begin{aligned}\Delta \Lambda^S(\theta, c) &= E_{\text{red}}^{SS}(\theta, c) \\ \Delta \Lambda^U(\theta, c) &= E_{\text{red}}^{UU}(\theta, c).\end{aligned}$$

On the other hand, the corrections of normal part of the change of basis

$P_\varepsilon(\theta, c)$, are obtained by iterating the systems

$$\begin{aligned} Q^{LS}(\theta, c) &= (\Lambda_\varepsilon^L(\theta, c)) (Q^{LS}(f(\theta, c))\Lambda_\varepsilon^S(\theta, c) - E_{\text{red}}^{LS}(\theta, c)) \\ Q^{LU}(\theta, c) &= \frac{\Lambda_\varepsilon^L(f^{-1}(\theta, c)) + E_{\text{red}}^{LU}(f^{-1}(\theta, c))}{\Lambda_\varepsilon^U(f^{-1}(\theta, c))} \\ Q^{US}(\theta, c) &= \frac{Q^{US}(f(\theta, c))\Lambda_\varepsilon^S(\theta, c) - E_{\text{red}}^{US}(\theta, c)}{\Lambda_\varepsilon^U(\theta, c)} \\ Q^{SU}(\theta, c) &= \frac{\Lambda_\varepsilon^S(f^{-1}(\theta, c))Q^{SU}(f^{-1}(\theta, c)) + E_{\text{red}}^{SU}(f^{-1}(\theta, c))}{\Lambda_\varepsilon^U(f^{-1}(\theta, c))}. \end{aligned}$$

3.2 Computation of bundles, maps and frames for the unperturbed case

We now derive semi-explicit expressions for the objects $f_0(\theta, c)$, $F_0(\theta, c, x, y, w)$, $DF_0(\theta, c)$ and $P_0(\theta, c)$. The expressions below have to be partially solved numerically. By semi-explicit we mean that we will assume that computations such as numerical integration or differentiation is exact.

For $\varepsilon = 0$, the map $F_0(\theta, c, x, y, w)$ consists of computing the stroboscopic map, integrating system (4), from t_0 to $t_0 + 2\pi/\omega$. However, we first need to compute the change of variables $p(\theta, c) = (u, v)$, which requires the computation of α_c . Note that the expression provided in Equation (8) implies computing an improper integral provided that $\dot{u} = 0$ at $u = u_1$, which is numerically problematic. Instead, we perform a Newton method to find the smallest $t^* > 0$ such that

$$\Pi_u(\varphi_{\mathcal{U}}(t^*; 0, \sqrt{2c})) = 0.$$

Then $\alpha_c = 2t^*$ due to the symmetry of the system. This is given by iterating the system

$$t_{i+1} = t_i - \frac{\Pi_u(\varphi_{\mathcal{U}}(t_i; 0, \sqrt{2c}))}{\Pi_v(\varphi_{\mathcal{U}}(t_i; 0, \sqrt{2c}))},$$

which allows to obtain very accurate solution (precision around 10^{-12} using order 7 – 8th order Runge Kutta integrator) in few iterations assuming that good enough first approximation is provided.

The stroboscopic map becomes

$$\mathfrak{s}_0(x, y, p(\theta, c), w) = \begin{pmatrix} \varphi_{\mathcal{X}}(2\pi/\omega; x, y) \\ \varphi_{\mathcal{U}}(\theta\alpha_c + 2\pi/\omega; 0, \sqrt{2c}) \\ w(2\pi/\omega; w) \end{pmatrix},$$

where $w(t; w)$ is the solution of equation

$$\dot{w} = -\lambda w - k(\Pi_y(\varphi_{\mathcal{X}}(t; x, y)) + \Pi_v(\varphi_{\mathcal{U}}(\tau; p(\theta, c)))). \quad (31)$$

Recall that, as mentioned in Section 2.1, Equation (31) can be seen as a one-dimensional non-autonomous differential equation, assuming that the flows $\varphi_{\mathcal{X}}$ and $\varphi_{\mathcal{U}}$ are known, but indeed depends on the initial values x, y, u, v . Writing \mathfrak{s} in variables θ, c , we obtain map F_0

$$F_0(\theta, c, x, y, w) = \begin{pmatrix} \theta + \frac{2\pi}{\omega\alpha_c} \\ c \\ \varphi_{\mathcal{X}}(2\pi/\omega; x, y) \\ w(2\pi/\omega; w) \end{pmatrix},$$

and we assume that we can integrate system \mathcal{X} and Equation (31) “exactly”. For $\varepsilon = 0$ the parameterization $K_0(\theta, c)$ becomes

$$K_0(\theta, c) = \begin{pmatrix} \theta \\ c \\ 0 \\ 0 \\ w_0^p(p(\theta, c)) \end{pmatrix}.$$

Again, we need to compute $w_0^p(p(\theta, c))$ numerically. One option is to numerically perform the integral given in Equation (20). However, it becomes faster and more precise to compute $w_0^p(p(\theta, c))$ as the solution of a fixed point equation. Recall that, when restricted to the manifold \tilde{K}_0 , (x, y) are kept constant to $(0, 0)$, and hence the dynamics is given by system \mathcal{U} and \dot{w} as given in Equation (10), which we write here for commodity

$$\left. \begin{aligned} \dot{u} &= v \\ \dot{v} &= \frac{1}{2}\beta u(1 - u^2) \\ \dot{w} &= \lambda w - kv \end{aligned} \right\}. \quad (32)$$

Let $\varphi_{\mathcal{U}w}(t; u, v, w)$ be the flow associated with system (32). Then, $w_0^p(p(\theta, c))$ is the solution for w_0 of the fixed point equation

$$\Pi_w(\varphi_{\mathcal{U}w}(\alpha_c; p(\theta, c), w_0)) - w_0 = 0, \quad (33)$$

which we can solve using a Newton method. Provided that α_c does not depend on w_0 , the derivative $\partial_{w_0}\Pi_w(\varphi_{\mathcal{U}w}(\alpha; p(\theta, c), w_0))$, necessary for the

Newton method, can be obtained by integrating the variational equations of system (32) from $t = 0$ to $t = \alpha_c$.

We next get

$$L_0(\theta, c) = DK_0(\theta, c) = \begin{pmatrix} 1 & 0 \\ 0 & 1 \\ 0 & 0 \\ 0 & 0 \\ \frac{\partial w_0^p(\theta, c)}{\partial \theta} & \frac{\partial w_0^p(\theta, c)}{\partial c} \end{pmatrix},$$

and we need to numerically compute the last row. Assuming that we have obtained $w_0^p(p(\theta, c))$, this can be done by applying the implicit function theorem to Equation (33), which leads to

$$\begin{aligned} \frac{\partial w_0^p(p(\theta, c))}{\partial \theta} &= - \frac{\overbrace{D_{uv}\Pi_w(\varphi_{\mathcal{U}w}(\alpha_c; u, v, w_0^p(u, v)))}_{(u,v)=p(\theta,c)} \cdot D_{\theta}p(\theta, c)}{\underbrace{\partial_{w_0}\Pi_w(\varphi_{\mathcal{U}w}(\alpha_c; p(\theta, c), w_0))}_{w_0=w_0^p(\theta,c)} - 1} \\ \frac{\partial w_0^p(p(\theta, c))}{\partial c} &= - \frac{\overbrace{\Pi_w(\varphi'_{\mathcal{U}w}(\alpha_c; p(\theta, c), w_0^p(p(\theta, c))))}_{-\lambda w_0^p(p(\theta,c)) - k\Pi_v(p(\theta,c))} \cdot \alpha'_c}{\partial_{w_0}\Pi_w(\varphi_{\mathcal{U}w}(\alpha_c; p(\theta, c), w_0))_{w_0=w_0^p(\theta,c)} - 1} - \\ &\quad - \frac{\overbrace{D_{uv}\varphi_{\mathcal{U}w}(\alpha_c; u, v, w_0^p(p(\theta, c)))}_{(u,v)=p(\theta,c)} \cdot D_cp(\theta, c)}{\underbrace{\partial_{w_0}\Pi_w(\varphi_{\mathcal{U}w}(\alpha_c; p(\theta, c), w_0))}_{w_0=w_0^p(\theta,c)} - 1}. \end{aligned}$$

The terms labeled with $*$ can be obtained by integrating the variational equations of system (32), so still to get expressions for α'_c and $D_{\theta c}p(\theta, c)$. The former one is obtained by finite differences provided that we can accurately compute α_{c+h} and α_{c-h} for a small enough $h > 0$. The latter becomes

$$\begin{aligned} Dp(\theta, c) &= D_{\theta,c}\varphi_{\mathcal{U}}(\theta\alpha_c; 0, \sqrt{2c}) \\ &= D_{uv}\varphi_{\mathcal{U}}(\theta\alpha_c; u, v)_{(u,v)=p(\theta,c)} \cdot \begin{pmatrix} 0 & 0 \\ 0 & \frac{1}{\sqrt{2c}} \end{pmatrix}, \end{aligned}$$

where $D_{uv}\varphi_{\mathcal{U}}(\theta\alpha_c; u, v)$ can be obtained integrating the variational equations associated with system \mathcal{U} .

We now compute

$$DF_0(\theta, c, x, y, w) = \begin{pmatrix} -\frac{\pi}{\omega\alpha_c^2}\alpha'_c & 1 & 0 & 0 & 0 \\ 0 & 1 & 0 & 0 & 0 \\ 0 & 0 & D_{xy}\varphi_{\mathcal{X}}(2\pi/\omega; x, y) & 0 & 0 \\ 0 & 0 & 0 & 0 & 0 \\ \partial_\theta w' & \partial_c w' & \partial_x w' & \partial_y w' & \partial_w w' \end{pmatrix},$$

where $w' = w(2\pi/\omega; w)$ is the solution of Equation (31) which, as emphasized above, depends also on θ, c, x, y . The first element of DF_0 requires computing α'_c , which we have already seen. The rest of the elements of DF_0 can be computed by integrating the full unperturbed system (4) together with its variational equations.

When evaluated at the manifold \tilde{K}_0 , the eigenvectors of DF_0 provides proper directions to split the normal space in stable and unstable directions and hence to obtain the matrix $N_0(\theta, c)$.

As shown in Lemma (1), at each point of the manifold \tilde{K}_0 the normal bundle is split in two stable directions and as unstable one. One stable direction is given by the contraction in w ; the other two are given by the stable and unstable directions of the saddle point Q_0 of system \mathcal{X} . These directions are given by the eigenvectors of matrix $DF_0(\tilde{K}_0)$

$$\begin{aligned} v_1^s &= (0, 0, 1, -1/\sqrt{2}, P_{5,3}) \\ v_2^s &= (0, 0, 0, 0, 1) \\ v^u &= (0, 0, 1, 1/\sqrt{2}, P_{5,5}), \end{aligned}$$

with

$$\begin{aligned} P_{5,3} &= \frac{1/\sqrt{2}\partial_y w' - \partial_x w'}{\partial_w w' + 1/\sqrt{2}} \\ P_{5,5} &= -\frac{1/\sqrt{2}\partial_y w' + \partial_x w'}{\partial_w w' - 1/\sqrt{2}}. \end{aligned}$$

Hence, $N_0(\theta, c)$ becomes

$$N_0(\theta, c) = \begin{pmatrix} 0 & 0 & 0 \\ 0 & 0 & 0 \\ 1 & 0 & 1 \\ -1/\sqrt{2} & 0 & 1/\sqrt{2} \\ P_{5,3} & 1 & P_{5,5} \end{pmatrix}.$$

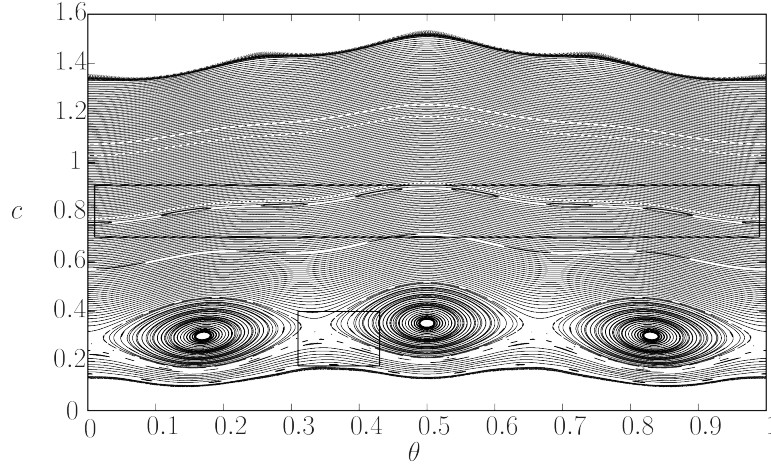


Figure 4: Inner dynamics in $\tilde{\mathcal{K}}_\varepsilon$ for the conservative case with $\varepsilon = 6 \cdot 10^{-2}$ obtained by iterating the numerically obtained map $f_\varepsilon(\theta, c)$.

4 Numerical results

We apply the method described in [18], Chapter 5, and summarized in Sections 3.1-3.2. We fix the following parameter values

$$\begin{aligned} G(t) &= \sin(\omega t) & \omega &= 2.1 \\ \lambda &= 0.02 & \tilde{\kappa} &= 1 \end{aligned}$$

and consider different situation regarding ε , $\tilde{\zeta}$ and $\tilde{\chi}$.

In all cases, we use as seed for the Newton method the unperturbed setting shown in Section 3.2 and use cubic spline interpolations in a grid of points for $(\theta, c) \in \mathbb{T} \times [0.1, 0.5]$. At each Newton step, the two substeps 3.1.1-3.1.2 are performed for each point of the grid, which allows a natural parallelization. This is done using “open mp” libraries and, ran in a 16 processors node, each Newton step takes around 2 minutes for a grid of 500×200 points. The code is available at

https://github.com/a-granados/nhim_parameterization

4.1 Conservative case

We start by setting $\tilde{\zeta} = \tilde{\chi} = 0$ and $\varepsilon = 6 \cdot 10^{-2}$.

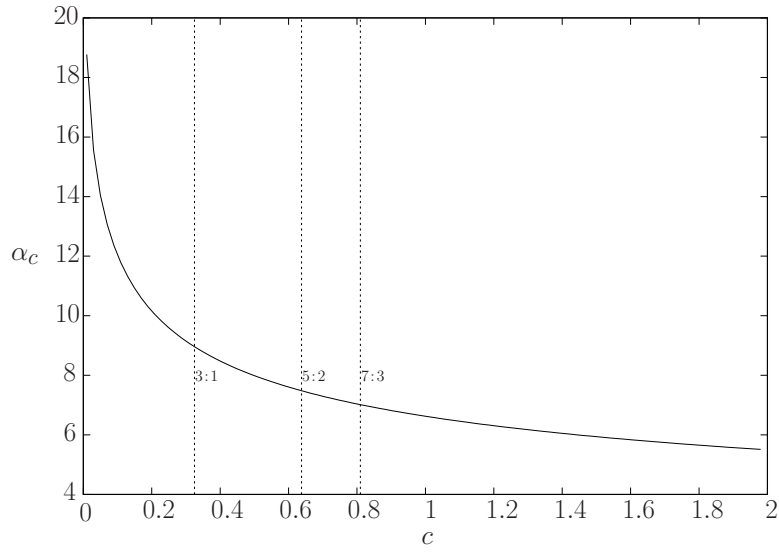


Figure 5: Periods of the unperturbed system, α_c . The labeled rectangles are magnified in Figures 6 and 7.

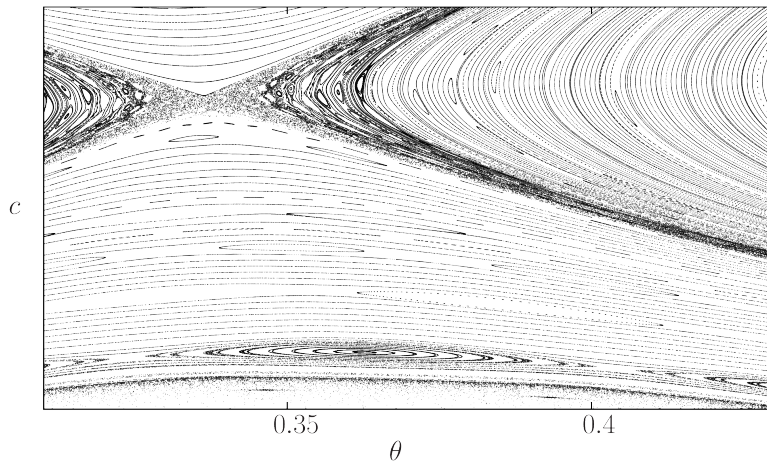


Figure 6: Blow up of the 3 : 1 resonance labeled in Figure 4

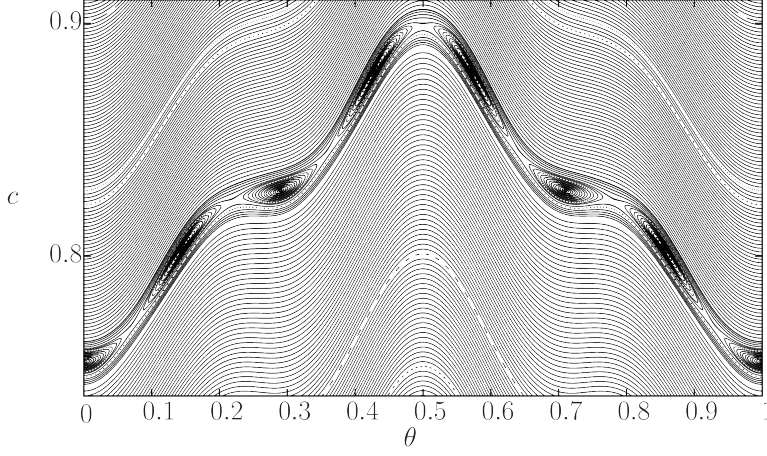


Figure 7: Blow up of the 7 : 3 resonance labeled in Figure 4

In this case, as mentioned above, the dynamics of the system restricted to $\tilde{\mathcal{K}}_\varepsilon$ becomes Hamiltonian. Moreover, for $\tilde{\zeta} = \tilde{\chi} = 0$ systems \mathcal{X} , \mathcal{U} and w remain uncoupled. The inner dynamics is given by the one and a half degrees of freedom Hamiltonian system, and f_ε becomes a symplectic map. In Figure 4 we show a global idea of the inner dynamics, where one can see typical objects of this type of maps. The space is mostly covered by KAM invariant curves acting as energy bounds. For the chosen value of ω one observes three main resonances: 3 : 1, 5 : 2 and 7 : 3, meaning $m : n$ that $mT = n\alpha_c$. They are labeled in Figure 5, where we show the periods of the unperturbed system as a function of c (α_c), and they approximately correspond to the unperturbed periodic orbits $\mathcal{P}_{0.325}$, $\mathcal{P}_{0.638}$ and $\mathcal{P}_{0.81}$ (see Equation 7 to remind the notation), respectively. As it comes from Melnikov theory for subharmonics orbits ([17]), when they persist, subharmonic periodic become an even number of periodic orbits of the stroboscopic map of the saddle and elliptic type; this number is given by the number of simple zeros of the so-called Melnikov function for subharmonic periodic orbits. In Figure ???? we show such function for these three resonances. Each of them possesses two simple zeros and, hence, there exist (for $\varepsilon > 0$ small enough) two periodic points of the stroboscopic map of the saddle and elliptic type. These periodic orbits are clearly observed for the 3 : 1 in Figure 4. The saddle type is magnified in Figure 6, where one also observes secondary tori and evidence of chaos given by the homoclinic tangles. The resonance 7 : 3 is magnified in Figure 7.

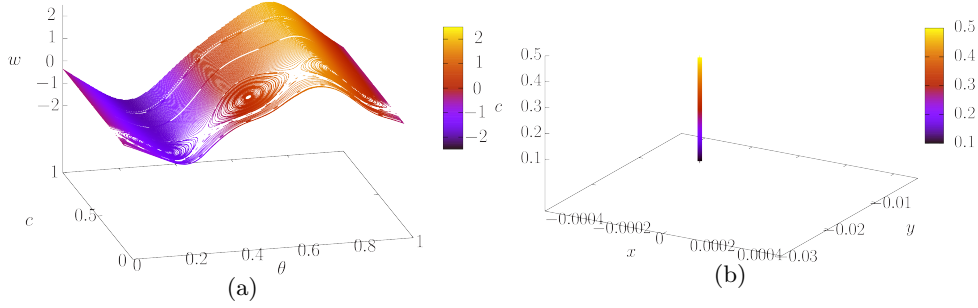


Figure 8: Dynamics restricted to the Normally Hyperbolic Manifold $\tilde{\mathcal{K}}_\varepsilon$ in the ambient space for the conservative case.

In Figure 8 we show the inner dynamics in the ambient space. In Figure 8(a) we show the variable w parameterized by θ and c . Note that it performs oscillations of increasing amplitude with c . These oscillations can be periodic or quasi-periodic depending on the dynamics of θ - c . In Figure 8(b) we see the behaviour of x and y . Note that, as system \mathcal{X} remains uncoupled and just periodically perturbed, the hyperbolic equilibrium point Q_0 becomes a T -periodic orbit and hence a fixed point of the time- T return time. Hence, in the latter figure one observes only a vertical line.

As explained in Section 3, the Newton-like method explained in [18] also provides corrected versions of the linearization of the stable and unstable bundles; that is, linear approximations of the parameterizations $W_\varepsilon^{s,\pm}$ and $W_\varepsilon^{u,\pm}$ given in Equations (23)-(24). In Figure 9 we show the $x - y - c$ projection of such approximations obtained by slightly varying, for each point at $\tilde{\mathcal{K}}_\varepsilon$, the two degrees of freedom of the stable leaf and one degree of freedom of the unstable one. Note that, hence, the stable bundle forms a volume, while the unstable one a tube. In Figure 10 we show the first 8 iterations of the linear approximations of stable and unstable bundles by f_ε^{-1} and f_ε , respectively.

Figure 10(a) shows evidence of homoclinic intersections. As the two beams remain uncoupled for $\tilde{\chi} = 0$, and the system is conservative, the energy, c , of system \mathcal{U} can only vary through the inner dynamics. Hence, such homoclinic

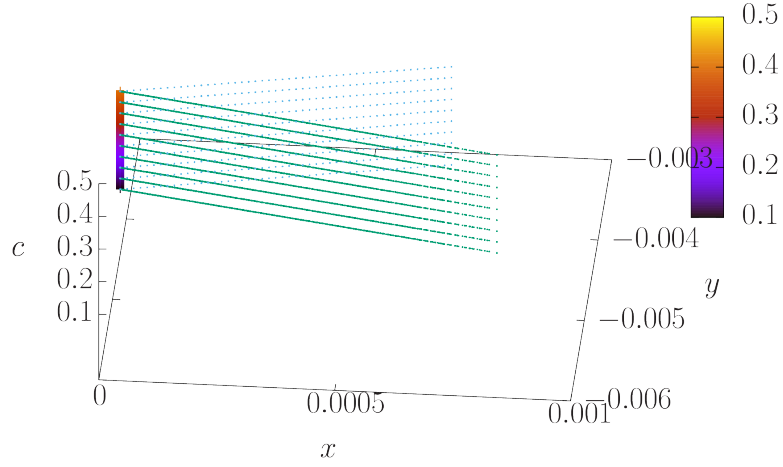


Figure 9: Tangent space to the stable (green) and unstable (blue) bundles

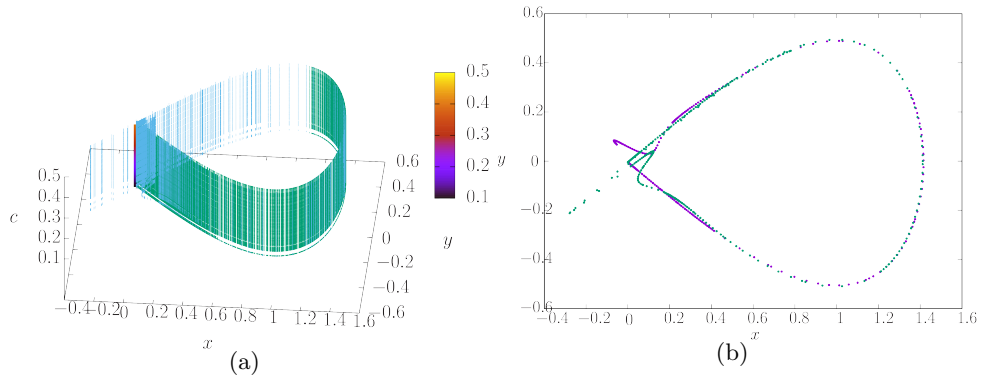


Figure 10: Iteration of the tangent spaces to the stable and unstable bundles shown in Figure 9.

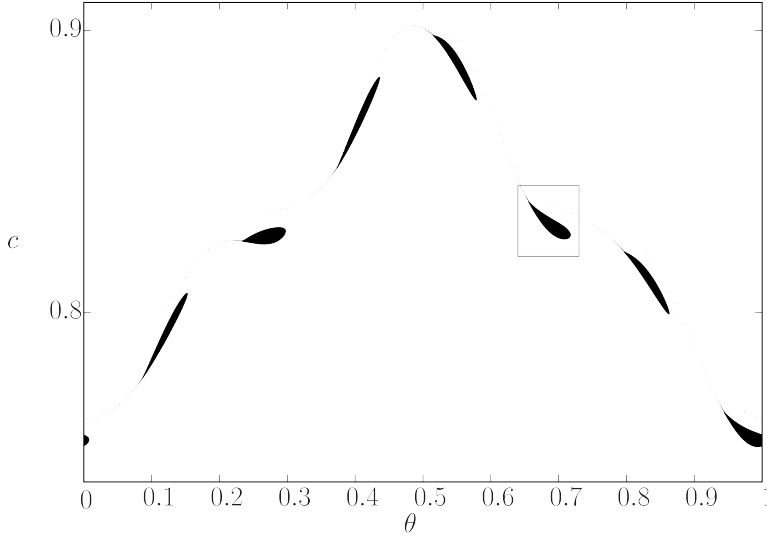


Figure 11: Approximated unstable manifold of the saddle periodic orbits corresponding to $7 : 3$ resonance under the presence of small damping, $\tilde{\chi} = 0$, $\tilde{\zeta} = 6 \cdot 10^{-5}$ and $\varepsilon = 6 \cdot 10^{-2}$. The unstable manifold leaves the saddle point and rolls about the $7 : 3$ resonant attracting focus. The labeled region is magnified in Figure 12(a).

excursions do not inject extra energy to the beam represented by system \mathcal{U} . In other words, the scattering map (see [7, 8]) becomes the identity up to first order terms and there is no hope to observe Arnold diffusion in this case.

4.2 Dissipative case

4.2.1 Weak damping

When adding small dissipation, hyperbolicity of the saddle periodic orbits guarantee their persistence for small enough dissipation. However, as shown in [24], when perturbed with dissipation, elliptic periodic orbits of area preserving maps become attracting foci. As shown in Figure 11, this occurs with f_ε as well. The elliptic periodic orbit corresponding to the $7 : 3$ resonance persists as an attracting focus when adding a small dissipation ($\tilde{\zeta} = 6 \cdot 10^{-5}$, which corresponds to absolute magnitude of the damping coefficient of $\varepsilon\tilde{\zeta} = 3.6 \cdot 10^{-6}$.) In Figure 11 we have taken an initial condition very close to the unstable manifold of the saddle periodic orbit. When it-

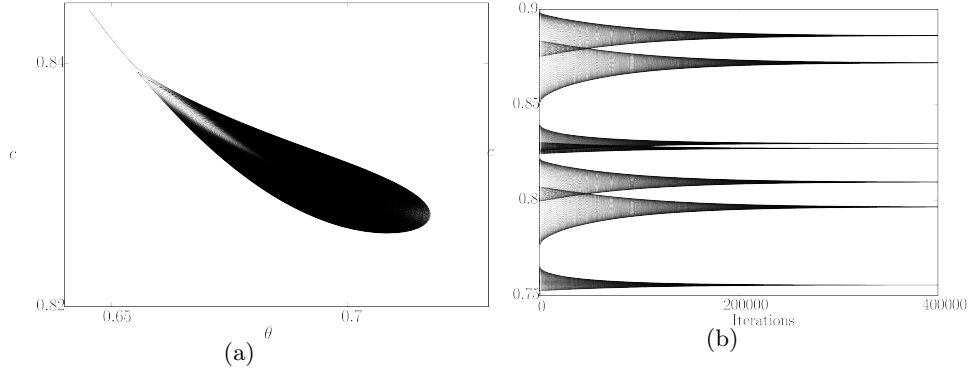


Figure 12: (a) blow up of the region labeled in Figure 11: unstable manifold of the 7 : 3 resonant periodic orbit under weak damping. (b) iterates of f_ε .

erated forwards, it rolls about the focus and, when iterated backwards, it escapes of after a few iterations. This is better observed in the magnification shown in Figure 12(a) and iterates shown in Figure 12(b).

4.2.2 Weak dissipative coupling

We now study the effect of adding a small dissipative coupling to the conservative system of Section 4.1.

Regarding the inner dynamics computations reveal that, as one would expect, the effect is similar to situation of Section 4.2.1 when only damping on the oscillators was considered. However, by contrast to the previous case, resonant periodic orbits persist for higher values of the dissipative parameter, in this case $\tilde{\chi}$.

In Figures 15 and 16(a) one can see that many of the resonances survive for $\tilde{\chi} = 10^{-4}$. As in the only-damping case, saddle periodic orbits persist while the elliptic ones become attracting foci. In Figure 16(b) we show the iterates of a point attracted by the 3 : 1-resonant focus. Note that backwards iterates are also shown until the trajectory escapes.

As shown in Figure 17, for larger values of $\tilde{\chi}$, periodic orbits bifurcate and most initial conditions are attracted towards a low energy attractor.

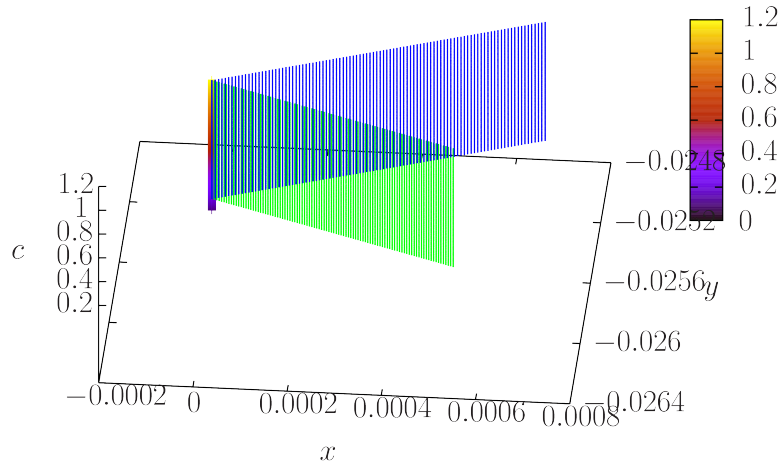


Figure 13: Local stable (green) and unstable manifolds (blue).

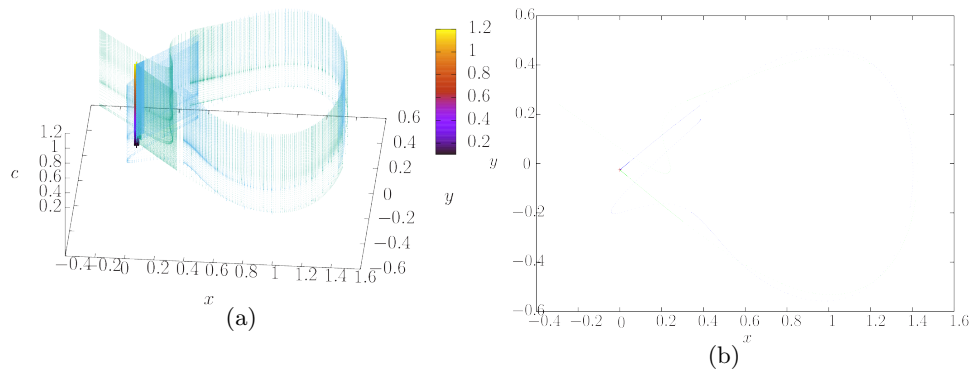


Figure 14: Iteration of the local stable (green) and unstable (blue) manifolds in the $x - y - c$ (a) and $x - y$ spaces.

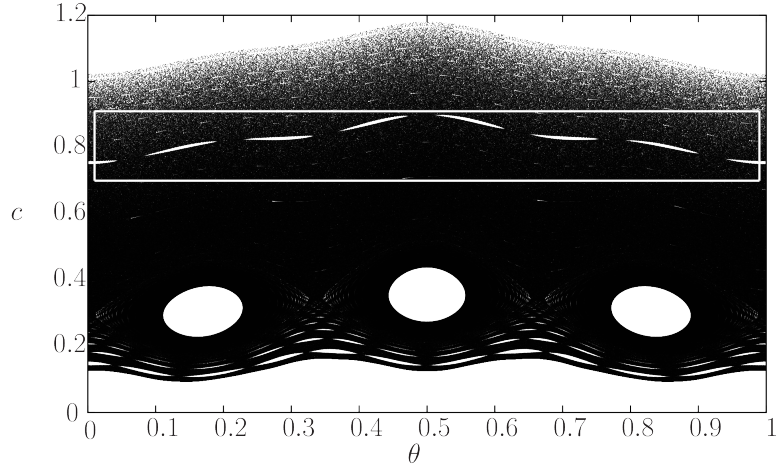


Figure 15: Inner dynamics in $\tilde{\mathcal{K}}_\varepsilon$ for weak dissipative coupling: $\varepsilon = 6 \cdot 10^{-2}$, $\tilde{\zeta} = 0$ and $\tilde{\chi} = 10^{-4}$.

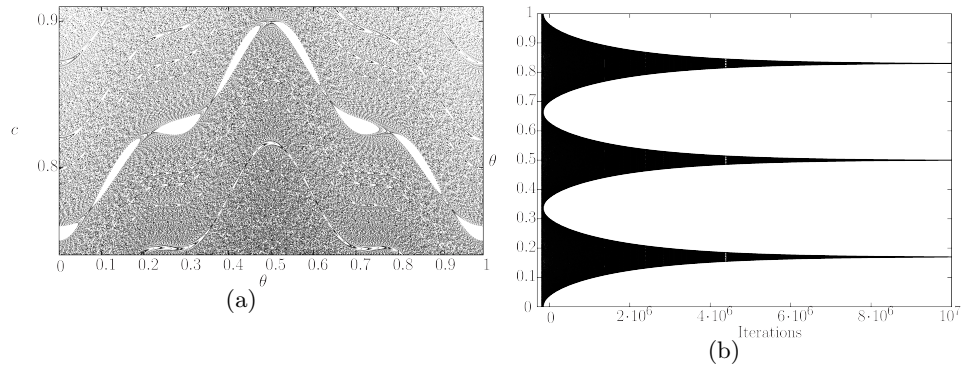


Figure 16: (a) Region labeled in Figure 15 magnified. (b) iterates by f_ε and f_ε^{-1} of an initial condition attracted by the 3-periodic focus.

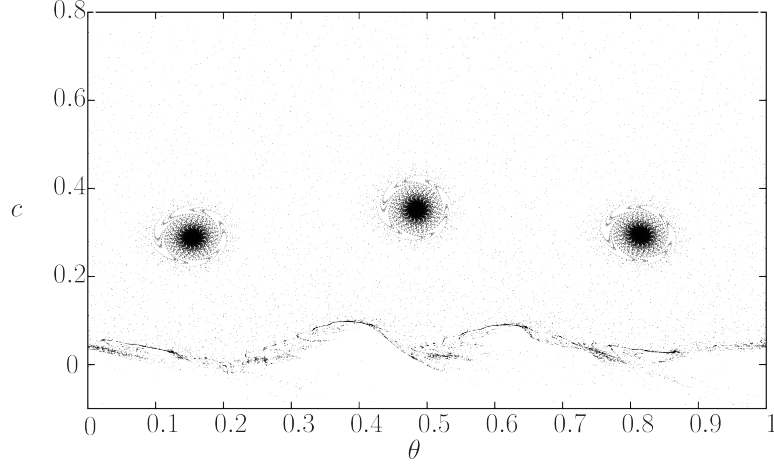


Figure 17: Inner dynamics for $\varepsilon = 6 \cdot 10^{-2}$, $\tilde{\zeta} = 0$ and $\tilde{\chi} = 2 \cdot 10^{-1}$.

For $\tilde{\chi} = 2 \cdot 10^{-1}$, the 3 : 1 resonant periodic attracting focus still exists.

In Figure 18 we show the dynamics restricted to $\tilde{\mathcal{K}}_\varepsilon$ in the ambient space. In the presence of coupling, the dynamics in the $x - y$ coordinates are not given by a T -periodic orbit anymore (fixed point of the stroboscopic map). In contrast to the conservative and damped cases studied in Sections 4.1 and 4.2.1, respectively, when $\tilde{\chi} > 0$ the map F_ε exhibits oscillations of amplitude $\varepsilon\tilde{\chi}$.

In Figure 19 we show the tangent spaces to the stable and unstable manifolds $W^s(\tilde{\mathcal{K}}_\varepsilon)$ and $W^u(\tilde{\mathcal{K}}_\varepsilon)$. When iterated by the global map F_ε defined in the ambient space, one obtains the results shown in Figure 20. As one can see, in Figure 20(b), there is evidence of the homoclinic intersections as well, which are generically persistent to perturbations due to their transversality. Due to the coupling between the beams, in this case homoclinic excursions may inject extra energy to system \mathcal{U} and lead to an increase the energy c . That is, the scattering may not have vanishing first order terms in ε . However, Arnold diffusion is unlikely to exist as the energy gain through homoclinic excursions may not be enough to compensate the loss of energy in the inner dynamics given by the dissipative nature of the coupling.

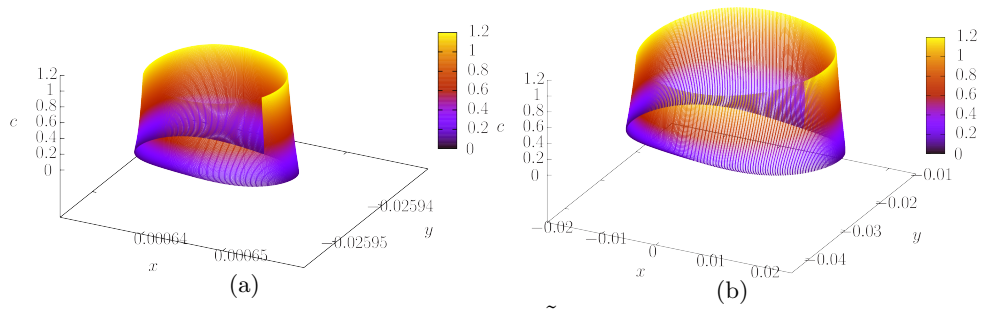


Figure 18: Normally Hyperbolic Manifold $\tilde{\mathcal{K}}_\epsilon$ in the ambient space. Parameter values are as in Figure 15 (a) and Figure 17 (b).

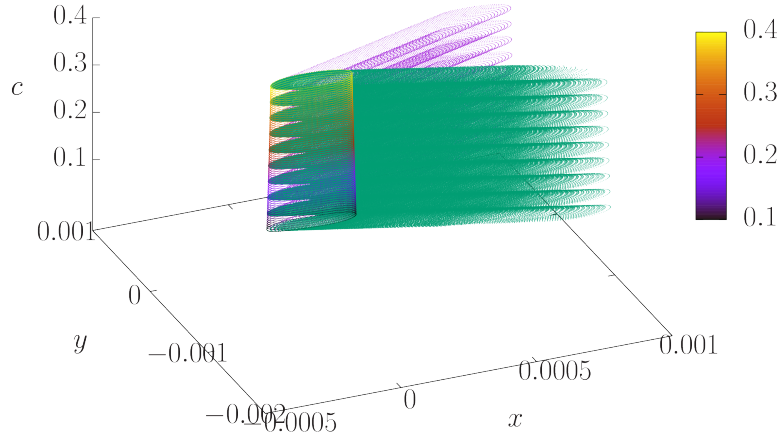


Figure 19: Tangent space to the stable (green) and unstable (blue) bundles in the presence of weak coupling.

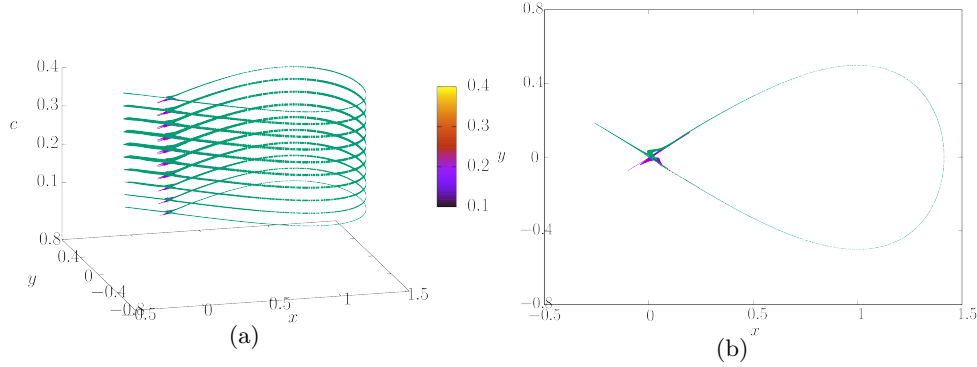


Figure 20: Iteration of the tangent spaces to the stable and unstable bundles shown in Figure 19.

References

- [1] V. I. Arnol'd. Instability of dynamical systems with several degrees of freedom. *Sov. Math. Doklady*, 5:581–585, 1964.
- [2] P. Bernard, V. Kaloshin, and K. Zhang. Arnol'd diffusion in arbitrary degrees of freedom and 3-dimensional normally hyperbolic invariant cylinders. *Acta Mathematica*, 2016. To appear.
- [3] X. Cabré, E. Fontich, and R. de la Llave. The parameterization method for invariant manifolds I: Manifolds associated to non-resonant subspaces. *Indiana Univ. Math. J.*, 52:283–328, 2003.
- [4] X. Cabré, E. Fontich, and R. de la Llave. The parameterization method for invariant manifolds II: Regularity with respect to parameters. *Indiana Univ. Math. J.*, 52:329–360, 2003.
- [5] X. Cabré, E. Fontich, and R. de la Llave. The parameterization method for invariant manifolds III: overview and applications. *J. Diff. Eqts.*, 218:444–515, 2005.
- [6] R. de la Llave. A tutorial on KAM theory. http://www.ma.utexas.edu/mp_arc-bin/mpa?yn=01-29, 2000.

- [7] A. Delshams, R. de la Llave, and T.M. Seara. A geometric mechanism for diffusion in hamiltonian systems overcoming the large gap problem: Heuristics and rigorous verification on a model. *Memoirs of the American Mathematical Society*, 179, 2006.
- [8] A. Delshams, R. de la Llave, and T.M. Seara. Geometric properties of the scattering map of a normally hyperbolic invariant manifold. *Adv. in Math.*, 217(3):1096–1153, February 2008.
- [9] A. Ertuk, J. Hoffman, and D.J. Inman. A piezomagnetoelastic structure for broadband vibration energy harvesting. *Applied Physics Letters*, 94, 2009.
- [10] A. Erturk and D.J. Inman. An experimentally validated bimorph cantilever model for piezoelectric energy harvesting from base excitations. *Smart Mater. Struct.*, 19, 2009.
- [11] A. Erturk, J.M. Renno, and D.J. Inman. Modeling of Piezoelectric Energy Harvesting from an L-saped Beam-mass Structure with an Application to UAVs. *Journ. Intell. Mat. Sys. Struc.*, 20, 2009.
- [12] J. Fejoz, M. Guardia, V. Kaloshin, and P. Roldan. Kirkwood gaps and diffusion along mean motion resonances in the restricted planar three-body problem. *Jour. Europ. Math. Soc.*, 2016. To appear.
- [13] N. Fenichel. Persistence and smoothness of invariant manifolds for flows. *Indiana Univ. Math. J.*, 21:193–226, 1971/1972.
- [14] M. Ferrari, V. Ferrari, M. Guizzetti, B. Andó, S. Baglio, and C. Trigona. Improved energy harvesting from wideband vibrations by nonlinear piezoelectric converters. *Procedia Chemistry*, 1(1):1203–1206, 2009.
- [15] M. Gidea, R. de la Llave, and T.M. Seara. A General Mechanism of Diffusion in Hamiltonian Systems: Qualitative Results. Preprint available at <http://arxiv.org/abs/1405.0866>, 2014.
- [16] A. Granados, S.J. Hogan, and T.M. Seara. The scattering map in two coupled piecewise-smooth systems, with numerical application to rocking blocks. *Physica D*, 269:1–20, 2014.
- [17] J. Guckenheimer and P. J. Holmes. *Nonlinear Oscillations, Dynamical Systems and Bifurcations of Vector Fields*. Appl. Math. Sci. Springer, 4th edition, 1983.

- [18] Àlex Haro, Marta Canadell, Josep-Lluís Figueras, Alejandro Luque, and Josep-Maria Mondelo. *The Parameterization Method for Invariant Manifolds: From Rigorous Results to Effective Computations*. Springer, 2016.
- [19] I.-H. Kim, H.J. Jung, B.M. Lee, and S.J. Jang. Broadband energy-harvesting using a two degree-of-freedom vibrating body. *Appl. Phys. Lett.*, 98, 2011.
- [20] G. Litak, M.I. Friswell, C.A. Kitio Kwiimy, S. Adhikari, and M. Borowiec. Energy harvesting by two magnetopiezoelectric oscillators. Proceedings of the XI conference on Dynamical Systems, Theory and Applications, Łódź December 2011, 2011.
- [21] A. Luque and D. Peralta-Salas. Arnold diffusion of charged particles in ABC magnetic fields. Preprint available at <http://arxiv.org/abs/1509.04141>, 2015.
- [22] J.-P. Marco. Arnold diffusion for cusp-generic nearly integrable systems on \mathbb{A}^3 . Preprint available at <http://arxiv.org/abs/1602.02403>, 2014.
- [23] F.C Moon and P.J. Holmes. A magnetoelastic strange attractor. *Journal of Sound and Vibration*, 65:275–296, 1979.
- [24] C. Simó and A. Viero. Planar radial weakly dissipative diffeomorphisms. *Chaos*, 20, 2010.
- [25] S.C. Stanton, B.A.M. Owens, and B.P. Mann. Harmonic balance analysis of the bistable piezoelectric inertial generator. *Journ. Sound Vibr.*, 331:3617–3627, 2012.
- [26] H. Vocca, I. Neri, F. Travasso, and L. Gammaitoni. Kinetic energy harvesting with bistable oscillators. *Applied Energy*, 97:771–776, 2012.